Mechanochromic Reconfigurable Metasurfaces

Artemios Karvounis*, Nikolaos Aspiotis, Ioannis Zeimpekis, Jun-Yu Ou, Chung-Che Huang, Daniel Hewak and N. I. Zheludev

Dr. A. Karvounis, Nikolaos Aspiotis, Dr. Ioannis Zeimpekis, Dr. Jun-Yu Ou, Dr. Chung-Che Huang, Prof. Dan Hewak, Prof. N. I. Zheludev
Optoelectronics Research Centre, University of Southampton, Southampton, SO17 1BJ, UK
Dr. A. Karvounis
Optical Nanomaterial Group, Institute for Quantum Electronics, ETH Zurich, 8093 Zurich, Switzerland
E-mail: karvounis@phys.ethz.ch
Prof. N. I. Zheludev
Centre for Disruptive Photonic Technologies & The Photonics Institute, School of Physical and Mathematical Sciences, Nanyang Technological University, Singapore 637371

Abstract:

The change of optical properties that some usually natural compounds or polymeric materials shown upon the application of external stress is named mechanochromism. Herein, an artificial nanomechanical metasurface formed by a subwavelength nanowire array made of Molybdenum Disulphide, Molybdenum oxide and Silicon nitride changes colour upon mechanical deformation. The aforementioned deformation induces reversible changes in the optical transmission (relative Transmission change of 197% at 654nm), thus demonstrating a giant mechanochromic effect. Moreover, these type of metasurfaces can exist in two non-volatile states presenting a difference in optical transmission of 45% at 678nm, when they are forced to bend rapidly. The wide optical tunability that photonic nano-mechanical metasurfaces, such as the one presented here, possess by design, can provide a valuable platform for mechanochromic and bistable responses across the visible and near infrared regime and form a new family of smart materials with applications in reconfigurable, multifunctional photonic filters, switches and stress sensors.

 Up to date, control of electromagnetic properties of photonic metamaterials and/or metasurfaces, artificial media structured on the subwavelength scale, have been achieved via

nanomechanical reconfiguration of its building blocks,[1–3] structural phase change in the material of constituting elements,[4–7] carrier injection effects,[8–11] application of liquid crystals,[12,13] chemical modification[14] and by stretching the elastic substrate supporting plasmonic or dielectric metamolecules.[15,16]

Mechanochromism is the colour change, upon mechanically induced reorganization of crystal structure or mechanically induced structural phase transition.[17] Such effects have been studied in a number of materials,[17,18] where strongest effects are seen in polymers,[19] liquid crystal elastomers,[20–22] nano-fibres[23] and photonic crystals.[24] Recently, chromic effects have been used as tuning mechanisms for photonic metasurfaces and plasmonics related devices with thermochromic and electrochromic responses, respectively.[25,26]

In recent years, strain engineering of optical and mechanical properties of solids, in particular silicon and two-dimensional solids have attracted considerable attention.[27–33] Two-dimensional materials, such as graphene, oxides, nitrides and transition metal dichalcogenides are of particular interest as constitutive elements for reconfigurable metamaterials and metasurfaces, as the extreme electron confinement inherits them with unique dielectric properties that can be controlled by external stimuli.[32,34]

In particular, molybdenum disulfide, MoS_2 is formed from the covalent bond between transition metal atoms (Mo) sandwiched by two layers of chalcogen atoms (Sulphur), while every sheet is bound via weak van der Waals interaction. Several theoretical reports have indicated that the energy bandgap renormalization can occur on MoS_2 upon stress, where microscopic parameters like carrier mobility and effective mass of carriers upon mechanical deformation can lead to substantial changes on refractive index. Furthermore, excitonic peak emission wavelengths have been observed to be sensitive to mechanical stress in its monolayer form.[35–40] MoS_2 has excellent mechanical properties because its large Young modulus (330GPa) and high elastic limit which makes it an attractive material for nanomechanical and mechanochromic devices.[41]

2

In this paper, we introduce a previously unexplored mechanism of tuning the optical properties of photonic metasurfaces that exploits the phenomenon of mechanochromism. We show that elastic strain in a MoS_2/ MoO_{3-x} /Si_3N_4 nanomechanical photonic metasurface causes a profound change in its optical properties, which originates from the strain-sensitive refractive index of MoS_2, enhanced by electromagnetic resonances created by nanostructuring. Specifically, heat activated nano-mechanical deformation of the array of nanowires lead to profound reversible changes of its transmission, reflection and absorption in the visible part of the spectrum operating either as a photonic filter or as a mechanically bistable element. Transmission changes up to 197% are obtained at 654nm upon 2% of mechanical strain, while two non-volatile states presenting a difference in optical transmission of 45% achieved at 675nm. The response of the system is controlled via the speed of induced mechanical stress. This type of devices can serve not only as photonic elements but also as strain sensors with an optical readout. Recently, more trilayer metasurfaces have been reported. [42]

The metasurface was fabricated on a 90nm thick Si_3N_4 membrane which was patterned as an array of nanowires 22μm long, 400nm wide with gaps of 100nm separating them (see **Figure 1**). The pre-patterned Si_3N_4 membrane, was coated with a 60nm thick layer of MoO_{3-x} and a 5nm layer of MoS_2 by atmospheric pressure chemical vapor deposition (APCVD). Figure 1a shows a top view of the metasurface, while the insets presents a cross-section of the trilayer film. The white dots seen on the SEM, are caused by the film growth and device fabrication process ; The short term roughness of the film is in the order of 1 MoS2 layer whereas the suspected contamination adds a waviness in the order of 3 nanometers (rms), verified by AFM measurements. The period of the contamination is in the order of 2-4 microns so this is beyond our wavelength of interest. The height of the individual contaminants is a maximum of 13 nm so with the refractive indices of our materials this translates to less than 1/10 of the wavelength of interest so it can be considered optically flat. More details related with TEM

and XRD analysis of MoS_2 films grown via APCVD method can be found in our previous publication[43], while the growth methods of the films are included in the experimental section.   The composition of the sample has been evaluated using reflective Raman spectroscopy. **Figure 1**b shows the Raman spectrum of the nanowire indicating its crystallinity: the 381 cm^{-1} line relates to the in-plane vibration mode, while the 407.5 cm^{-1} line corresponds to the out-of-plane vibration A_{1g} mode of MoS_2.[44] The 353 cm^{-1} and 733 cm^{-1} lines indicate the presence of MoO_{3-x} in the structure. [45] Furthermore, we measured the complex refractive index of MoS_2 layer of the composite nanomembrane by spectral ellipsometry, **Figure 1**c. The refractive index of our films is similar to previous literature,[46] demonstrating MoS_2 as a high index dielectric material. These results were used to computationally model the optical properties of the nanowire array, as presented in **Figure 2**b. Measured and computed optical properties of the metamaterial are presented in **Figure 2.** At optical wavelengths longer than the structure period of 500nm the nanowire array does not scatter light and acts as an optically homogeneous metamaterial layer, that can be fully characterized in terms of its transmission, reflection and absorption. However, the periodic structuring, results in reflection and transmission resonances at 654nm and 810nm for linearly polarized light parallel to the wires, with a quality factor of Q~25. The experimental spectra are well reproduced in computational modelling, as shown in **Figure 2b**. The field maps in **Figure 2c,d** reveal that on resonance, displacement currents running through the nanowires with a higher concentration within the high index MoS_2 part, interfere constructively with incident light and block transmission over this wavelength, as studied in the past.[6,47,48] Small discrepancies between measured and computed spectra can be attributed to fabrication tolerances and accuracy of the refractive index values used in the modelling.

Optical properties of such metasurfaces are expected to be strongly dependent on temperature, given the stress-induced modifications of the band structure of MoS_2 component. Indeed, heat activated nanoscale reconfiguration of the metamaterial induces nanomechanical deformation

4

of the wires. Since the MoS_2 is much thinner than Si_3N_4 and MoO_{3-x} layers, the thermal

expansion mismatch between the Si_3N_4 and MoO_{3-x} is the main mechanism of the bow-like

deformation of the nanowires upon cooling/heating (the thermal expansion coefficients are 2

x 10^{-6} K^{-1} and 6 x 10^{-5} K^{-1} [49], respectively). This deformation in its own turn leads to the

stress-induced modification of the optical properties of the MoS_2 layer. Stress-induced change

of optical properties of the wide band gap materials Si_3N_4 (E_g = 4.5eV)[50] and MoO_{3-x} (E_g=

3.1eV)[51] is insignificant in the part of the spectrum of interest.

Our finite element method (FEM) mechanical stress calculations -based on the linear

momentum balance equation and the linear stress-strain relation- are displayed in **Figure 1d**,

employing a single nanowire. Strain ε is the ratio of the deflection of the MoS2 layer from

the neutral plane, y over the radius of curvature, R, ε=y/R. They show that the decrease of the

temperature on a nanowire array from 300K to 110K results in a bow-like deformation of

50nm that induces a compressive stress of 2.05% to the MoS_2 layer. This is a finite element

method simulation, as a result stress levels may differ upon grown methods of the films and

nanostructuring techniques.

Since thermal cooling of the metasurface induces mechanical strain upon the MoS_2 layer, the

transmission spectra were measured at different temperatures using a

microspectrophotometer, to test its mechanochromic response. We first studied the induced

changes in optical transmission as a function of applied strain. **Figure 3** presents the optical

transmission of the mechanochromic metasurface for various strain levels, at the cooling rate

of 5K/min. We define the relative transmission change *ΔT/T₀*, where *ΔT = T_ε - T_0*; *T_ε* being the

absolute transmission at an applied strain *ε* and *T_0* the transmission for zero strain. For small

strain levels –below 1%- the transmission change is small, however larger strain upon MoS_2

induces change in Transmission spectra of the sample. At 2% strain the induced change

reaches maximum values of 197% and 80% at 657 and 810 nm, accompanied with the

sample's colour change, inset **Figure 3a**. Since, some semiconductors show a variation of

their bandgap with temperature, we test if the response in colour change is related with the amount of stress applied on the metasurface, or due to temperature. **Figure 3b** shows the relative transmission difference of the metasurface, for several levels of stress reaching up to 200%, while the trilayer films, where no elastic strain exist, provide transmission changes of the level of 2% between room temperature and 110K as shown in the inset of **Figure 3.** Furthermore, no change of the lineshape is recorded, since the relative change is flat. In this work, we did not study the limits of elastic deformation and therefore we did not exceed the 2% applied strain level in pursuit of higher transmission change to avoid irreversible nanomechanical deformations. This performance is already exceptionally high as the metasurface's transmission minimum shifts from λ_o=657nm to λ_1=681nm –providing giant mechanochromic sensitivity, which is defined by the ratio of the wavelength shift over the applied strain $\Delta\lambda/\varepsilon$ [nm/%] and is found to be as high as 12, one order of magnitude larger than other polymeric mechanochromic systems.[24] More interestingly, our device outperforms recent reports on polymer based mechanochromic devices.[21] The mechanochromic metasurface demonstrates transmission difference of 200% under 2% strain at 645 nm wavelength. In contrast, in [21] ; on Fig 1h it is recorder 77% transmission difference under 50% strain at the wavelength of 600 nm, thus our work outperforms on the transmission contrast achieved. At this and slower cooling rates the change in transmission do not show any hysteretic response.

Upon a faster cooling rate, 15K/min, a hysteretic behavior of metamaterial's transmission is observed. **Figure 4a** presents a selection of spectra for different strain levels. For increasing strain, the metasurface demonstrates a red-shift of its spectrum similar to **Figure 3**. However, on the level of 1.9% strain the second dip of transmission mode is recorded, as transmission jumps from 31% to 41% for the wavelength of 680nm, see **Figure 4b**. In **Figure 4b** we show the full strain cycle over transmission at the wavelength of 680nm. Upon decreasing strain – blue line- the optical spectra are different from those of the same strain level for increasing

strain- red line. At the level of 1% strain the hysteretic loop closes. Furthermore, we define

the differential hysteresis: $\Delta h = Abs[Tr_{up}(\lambda)-Tr_{down}(\lambda)]/Tr_{up}(\lambda)$

as the relative transmission difference between the two non-volatile states for increasing-

decreasing strain, with the largest value recorded at the wavelength of 678nm equal to 47%.

This response is mainly driven by the mechanical buckling of the metasurface;[52,53] an effect

accompanying flexible parts when subject to large applied mechanical load and therefore

demonstrate mechanical bistability.

The experimentally observed red-shift of the optical response of the metamaterial spectrum

depending on temperature can be satisfactorily explained in terms of mechanocromism. The

red-shift of the spectrum is related to the mechanochromic nature of device rather than the

structural reconfiguration of the sample. We have designed the metamaterial to keep its

optical response invariant upon deflection of the nanowires. Upon cooling, nanowires bend in

the same fashion, as a result, the metamaterial's response is expected to provide negligible

transmission changes for small deformations between neighboring nanowires, since most

parameters remain the same such as the distance between the nanowires and the period of the

metasurface. This is in contrast to previous works that present substantial changes in the

optical properties due to the doubling of metamaterial's period or by controlling the gap

between the nanowires.[1,54,55] Our mechanical FEM calculations (COMSOL) indicate that the

mid-point of each nanowire is displaced out-of-plane by ~50 nm when strain is at 2% and

temperature at 110K. For this deflection, the optical FEM modelling indicates that solely the

50nm mechanical deformation of the central part of the array of the nanowires can induce

relative transmission changes smaller than 5%, see **Figure 3c**. Moreover, the simulation

without MoS_2 film reveals a similar response with Figure 3c, with the transmission difference

at 645nm to be less than 3%, in contrast to experimentally observed change of 200%, at

Figure 3b. Furthermore, the fact that the transmission change is nonlinear with the applied

strain, **Figure3d** as well as the observed hysteresis related to the applied stress rate over an

increasing-decreasing thermal cycle, **Figure 4**, further verifies the mechanical nature of the effect over any thermal effects, that might exist, negligible in the current study.

In summary, we have reported a new mechanism to tune the optical properties of photonic metamaterials. We have studied the mechanochromic response of MoS_2 metasurfaces and identified the conditions under which they can operate either as photonic filters or switches. The proposed device provides continuous and reversible optical tuning of visible transmission with relative transmission change of more than 190% actuated by a strain level of 2%, which is translated into great mechanochromic sensitivity. For example, materials with larger thermal expansion coefficient difference or longer nanowires can improve mechanochromic sensitivity. Moreover, new designs of mechanochromic metasurfaces should be developed to improve the bandwidth of the response. Even though we apply a heat-actuated method to induce stress on the mechanochromic metasurfaces, equivalent strain effects are also achievable via electrically means in nanomechanical metamaterials, such as electrostriction.[56] We also believe that other types of transition metal dichalcogenides should be studied as strain dependent refractive index materials for metamaterials, targeting different operational wavelengths. Overall, the use of photonic metasurface technology for creating mechanochromic devices based on transition metal dichalcogenides, can be used as a general platform for force responsive materials with optical readouts and form a new family of ultrathin colour displays and multifunctional devices.

Experimental section

Metamaterial fabrication: Nano-grating metamaterial patterns, with a fixed gap width g=100 nm and period P=500 nm, covering an area of approximately 22μm x 25μm, were directly etched via focused ion beam (FIB) milling, using a FEI Helios NanoLab 600 dual beam system, on a commercially available 90nm thick Si_3N_4 membrane from Norcada Inc. Then, an APCVD synthesis method was used for the deposition of the MoS_2 on the pre-patterned

8

membrane, with two separate precursors: MoO_3 and sulphur loaded in two 3cm quartz tubes in a CVD chamber. A silicon nitride membrane is placed at the centre of the furnace and a quartz boat containing the MoO_3 precursor was placed upstream at a distance of 3cm. The sulphur powder is placed in a separate quartz boat outside the furnace at a distance of 30cm with controlled ambient temperature. Prior to the deposition, the quartz tube was flushed with 500sccm of Ar gas for 1h. The temperature of the furnace was first ramped up to 500°C with a rate of 20 °C / min and subsequently up to 700°C with 4°C/min under constant flow of Ar at 200sccm allowing the evaporation and deposition of MoO_3. At the temperature of 700°C the sulphur zone was heated up to 170°C for 15 minutes. During the process, a sulphur rich time window, the as-deposited MoO_3 was partially converted to MoO_{3-x} and MoS_2 progressing in a layer by layer manner while MoS_2 in the gas phase is co–deposited. After the 15 minutes time window, the gradually sulphur deficient environment results in the deposition of a metal oxide rich layer.

Variable-Angle Spectroscopic Ellipsometry: The complex relative permittivity/refractive index APCVD deposited MoS_2 was evaluated by spectroscopic ellipsometry (J. A. Woollam 4000) over the wavelength range from 400 to 900 nm.

Numerical simulations: Full-wave electromagnetic simulations of the metamaterial structure, based on the geometry presented in **Figure 1a**, were performed using the finite element method in COMSOL Multiphysics. Calculations employ periodic boundary conditions in the *x* and *y* directions (i.e. effectively assuming an infinite array of infinitely long nanowires). They utilize refractive indices for silicon nitride and MoO_{3-x} assumed to be non-dispersive and equal to 2, while for MoS_2 ellipsometry data used are presented in **Figure 1c**. Furthermore, numerical spectra are integrated over the numerical aperture of the objective in the experiment, assuming linearly polarized plane wave illumination; Nanowire mechanical deformation was obtained from finite element models of a single, isolated 22μm long wire with fixed ends and rectangular cross sections as presented in **Figure 1**. These assumed

Young's moduli E and density ρ values for Si_3N_4, MoO_{3-x} and MoS_2: E_{SiN} = 200 GPa; E_{MoO} = 80 GPa; E_{MoS}=320 GPa; ρ_{SiN} = 3170 kg m^{-3}, ρ_{MoO} = 4690 kg m^{-3}, ρ_{MoS}=5060 kg m^{-3}.

Raman spectroscopy: Raman measurements under 532nm laser excitation indicate the deposition on the prepatterned membrane of both MoO_{3-x} and MoS_2. The bulk MoS_2 was confirmed by the Raman mode at ~381 cm^{-1} and A_{1g} mode at 407.5 cm^{-1};[44] and the MoO_{3-x} the Raman peaks at 353 cm^{-1} and 733 cm^{-1}. [45]

Microspectrophotometry (including low temperature measurements): transmission and reflection spectra (**Figure 2**) were obtained using a microspectrophotometer (CRAIC QDI2010), with a 11µm × 11µm sampling aperture via a 15× objective with NA 0.28. All data are normalized to reference levels for air (100% transmission), a silver mirror (high reflector) and a 'Vantablack' vertically-aligned carbon nanotube array (zero reflection/ transmission), and averaged over 15 repeated measurement cycles, each with a 500ms integration time. For the low temperature measurements, a cryogenic Linkam stage (model No THMS600) with temperature control. Pressure level is monitored throughout the experiment at 10^{-3} mbar. Measurements performed while temperature level was stabilized with fluctuation of less than 0.1K;

Acknowledgements

Received: ((will be filled in by the editorial staff))

Revised: ((will be filled in by the editorial staff))

Published online: ((will be filled in by the editorial staff))

References:

[1]   J. Y. Ou, E. Plum, L. Jiang, N. I. Zheludev, *Nano Lett.* **2011**, *11*, 2142.

[2]   A. Karvounis, J.-Y. Ou, W. Wu, K. F. MacDonald, N. I. Zheludev, *Appl. Phys. Lett.* **2015**, *107*, 191110.

[3]   J. Canet-Ferrer, A. Afridi, L. Philippet, R. Quidant, J. Osmond, P. Berto, *ACS Photonics* **2018**, *5*, 4497.

[4]   T. Driscoll, H.-T. Kim, B.-G. Chae, B.-J. Kim, Y.-W. Lee, N. M. Jokerst, S. Palit, D. R. Smith, M. Di Ventra, D. N. Basov, *Science (80-.).* **2009**, *325*, 1518.

[5]   A. Tittl, A. K. U. Michel, M. Sch??ferling, X. Yin, B. Gholipour, L. Cui, M. Wuttig, T. Taubner, F. Neubrech, H. Giessen, *Adv. Mater.* **2015**, *27*, 4597.

[6]   A. Karvounis, B. Gholipour, K. F. Macdonald, N. I. Zheludev, *Appl. Phys. Lett.* **2016**, *109*, 051103.

[7]   Q. Wang, E. T. F. Rogers, B. Gholipour, C.-M. Wang, G. Yuan, J. Teng, N. I. Zheludev, *Nat. Photonics* **2016**, *10*, 60.

[8]   K. M. Dani, Z. Ku, P. C. Upadhya, R. P. Prasankumar, S. R. J. Brueck, A. J. Taylor, *Nano Lett.* **2009**, *9*, 3565.

[9]   M. Ren, B. Jia, J. Ou, E. Plum, J. Zhang, K. F. Macdonald, A. E. Nikolaenko, J. Xu, M. Gu, N. I. Zheludev, *Adv. Mater.* **2011**, *23*, 5540.

[10]   Y.-W. Huang, H. W. H. Lee, R. Sokhoyan, R. A. Pala, K. Thyagarajan, S. Han, D. P. Tsai, H. A. Atwater, *Nano Lett.* **2016**, *16*, 5319.

[11]   M. Morea, K. Zang, T. I. Kamins, M. L. Brongersma, J. S. Harris, *ACS Photonics* **2018**, *5*, 4702.

[12]   A. Minovich, J. Farnell, D. N. Neshev, I. McKerracher, F. Karouta, J. Tian, D. A. Powell, I. V Shadrivov, H. Hoe Tan, C. Jagadish, Y. S. Kivshar, *Appl. Phys. Lett.* **2012**, *100*, 121113.

[13] O. Buchnev, J. Y. Ou, M. Kaczmarek, N. I. Zheludev, V. a Fedotov, *Opt. Express* **2013**, *21*, 1633.

[14] F. Sterl, N. Strohfeldt, R. Walter, R. Griessen, A. Tittl, H. Giessen, *Nano Lett.* **2015**, *15*, 7949.

[15] I. M. Pryce, K. Aydin, Y. A. Kelaita, R. M. Briggs, H. A. Atwater, *Nano Lett.* **2010**, *10*, 4222.

[16] P. Gutruf, C. Zou, W. Withayachumnankul, M. Bhaskaran, S. Sriram, C. Fumeaux, *ACS Nano* **2016**, *10*, 133.

[17] M. K. Beyer, H. Clausen-schaumann, **2005**, *105*, DOI 10.1021/cr030697h.

[18] J. X. X. Zhang, Z. Chi, Y. Zhang, S. Liu, *J. Mater. Chem. C* **2013**, 3376.

[19] B. R. Crenshaw, C. Weder, *Chem. Mater.* **2003**, *15*, 4717.

[20] E. Lee, M. Zhang, Y. Cho, Y. Cui, J. Van Der Spiegel, N. Engheta, S. Yang, *Adv. Mater.* **2014**, *26*, 4127.

[21] S. Zeng, D. Zhang, W. Huang, Z. Wang, S. G. Freire, X. Yu, A. T. Smith, E. Y. Huang, H. Nguon, L. Sun, *Nat. Commun.* **2016**, *7*, 11802.

[22] E. Ducrot, Y. Chen, M. Bulters, R. P. Sijbesma, C. Creton, *Science (80-.).* **2014**, *344*, 186.

[23] M. Raisch, D. Genovese, N. Zaccheroni, S. B. Schmidt, M. L. Focarete, M. Sommer, C. Gualandi, *Adv. Mater.* **2018**, *30*, 1802813.

[24] E. P. Chan, J. J. Walish, A. M. Urbas, E. L. Thomas, *Adv. Mater.* **2013**, *25*, 3934.

[25] K. Sun, C. A. Riedel, A. Urbani, M. Simeoni, S. Mengali, M. Zalkovskij, B. Bilenberg, C. H. De Groot, O. L. Muskens, *ACS Photonics* **2018**, *5*, 2280.

[26] G. J. Stec, A. Lauchner, Y. Cui, P. Nordlander, N. J. Halas, *ACS Nano* **2017**, *11*, 3254.

[27] A. Castellanos-Gomez, R. Roldán, E. Cappelluti, M. Buscema, F. Guinea, H. S. J. Van Der Zant, G. A. Steele, *Nano Lett.* **2013**, *13*, 5361.

[28] N. Papasimakis, S. Mailis, C. C. Huang, D. W. Hewak, Z. Luo, Z. X. Shen, **2015**,

061904, 7.

[29] X. Fu, C. Su, Q. Fu, X. Zhu, R. Zhu, C. Liu, Z. Liao, J. Xu, *Adv. Mater.* **2014**, *26*, 2572.

[30] H. Gao, Q. Shi, D. Rao, Y. Zhang, J. Su, Y. Liu, Y. Wang, K. Deng, R. Lu, *J. Phys. Chem. C* **2017**, *121*, 22105.

[31] Q. Guo, Z. Di, M. G. Lagally, Y. Mei, *Mater. Sci. Eng. R* **2018**, *128*, 1.

[32] Y. Zhang, W. Liu, Z. Li, H. Cheng, Y. Zhang, G. Jia, S. Chen, J. Tian, *Appl. Phys. Lett.* **2017**, *111*, DOI 10.1063/1.4992045.

[33] S. Chen, Z. Li, W. Liu, H. Cheng, J. Tian, *Adv. Mater.* **2019**, *31*, 1.

[34] G. V. Naik, V. M. Shalaev, A. Boltasseva, *Adv. Mater.* **2013**, *25*, 3264.

[35] Y. Li, Z. Zhou, S. Zhang, Z. Chen, *J. Am. Chem. Soc.* **2008**, *130*, 16739.

[36] L. Kou, C. Tang, Y. Zhang, T. Heine, C. Chen, T. Frauenheim, *J. Phys. Chem. Lett.* **2012**, *3*, 2934.

[37] P. Johari, V. B. Shenoy, *ACS Nano* **2012**, *6*, 5449.

[38] H. Peelaers, C. G. Van de Walle, *Phys. Rev. B* **2012**, *86*, 241401.

[39] L. Yang, X. Cui, J. Zhang, K. Wang, M. Shen, S. Zeng, S. A. Dayeh, L. Feng, B. Xiang, *Sci. Rep.* **2014**, *4*, 5649.

[40] F. Kafi, R. Pilevar Shahri, M. R. Benam, A. Akhtar, *J. Electron. Mater.* **2017**, *46*, 6158.

[41] A. Castellanos-gomez, M. Poot, G. A. Steele, H. S. J. Van Der Zant, *Adv. Mater.* **2012**, *24*, 772.

[42] B. Yang, W. Liu, Z. Li, H. Cheng, D. Y. Choi, S. Chen, J. Tian, *Nano Lett.* **2019**, *19*, 4221.

[43] C. C. Huang, F. Al-Saab, Y. Wang, J. Y. Ou, J. C. Walker, S. Wang, B. Gholipour, R. E. Simpson, D. W. Hewak, *Nanoscale* **2014**, *6*, 12792.

[44] C. Lee, H. Yan, L. Brus, T. Heinz, J. Hone, S. Ryu, *ACS Nano* **2010**, *4*, 2695.

[45] M. Dieterle, G. Mestl, *Phys. Chem. Chem. Phys.* **2002**, *4*, 822.

[46] C. Yim, M. O'Brien, N. McEvoy, S. Winters, I. Mirza, J. G. Lunney, G. S. Duesberg, *Appl. Phys. Lett.* **2014**, *104*, DOI 10.1063/1.4868108.

[47] B. Gholipour, G. Adamo, D. Cortecchia, H. N. S. Krishnamoorthy, M. D. Birowosuto, N. I. Zheludev, C. Soci, *Adv. Mater.* **2017**, *29*, 1.

[48] B. Gholipour, D. Piccinotti, A. Karvounis, K. F. Macdonald, N. I. Zheludev, **2019**, DOI 10.1021/acs.nanolett.8b04576.

[49] S. K. Deb, *Proc. Roy. Soc. A* **1968**, *304*, 211.

[50] Y.-N. Xu, W. Y. Ching, *Phys. Rev. B* **1995**, *51*, 379.

[51] W. Yang, Z. Wei, X. Zhu, D. Yang, *Phys. Lett. A* **2009**, *373*, 3965.

[52] J. W. Jiang, *Nanotechnology* **2014**, *25*, 355402.

[53] S. K. Singh, M. Neek-Amal, S. Costamagna, F. M. Peeters, *Phys. Rev. B* **2015**, *91*, 14101.

[54] J. Valente, J.-Y. Ou, E. Plum, I. J. Youngs, N. I. Zheludev, *Nat. Commun.* **2015**, *6*, 7021.

[55] Y. Nagasaki, B. Gholipour, J.-Y. Ou, M. Tsuruta, E. Plum, K. F. MacDonald, J. Takahara, N. I. Zheludev, *Appl. Phys. Lett.* **2018**, *113*, 21105.

[56] A. Karvounis, B. Gholipour, K. F. MacDonald, N. I. Zheludev, *Adv. Mater.* **2019**, *31*, 1804801.
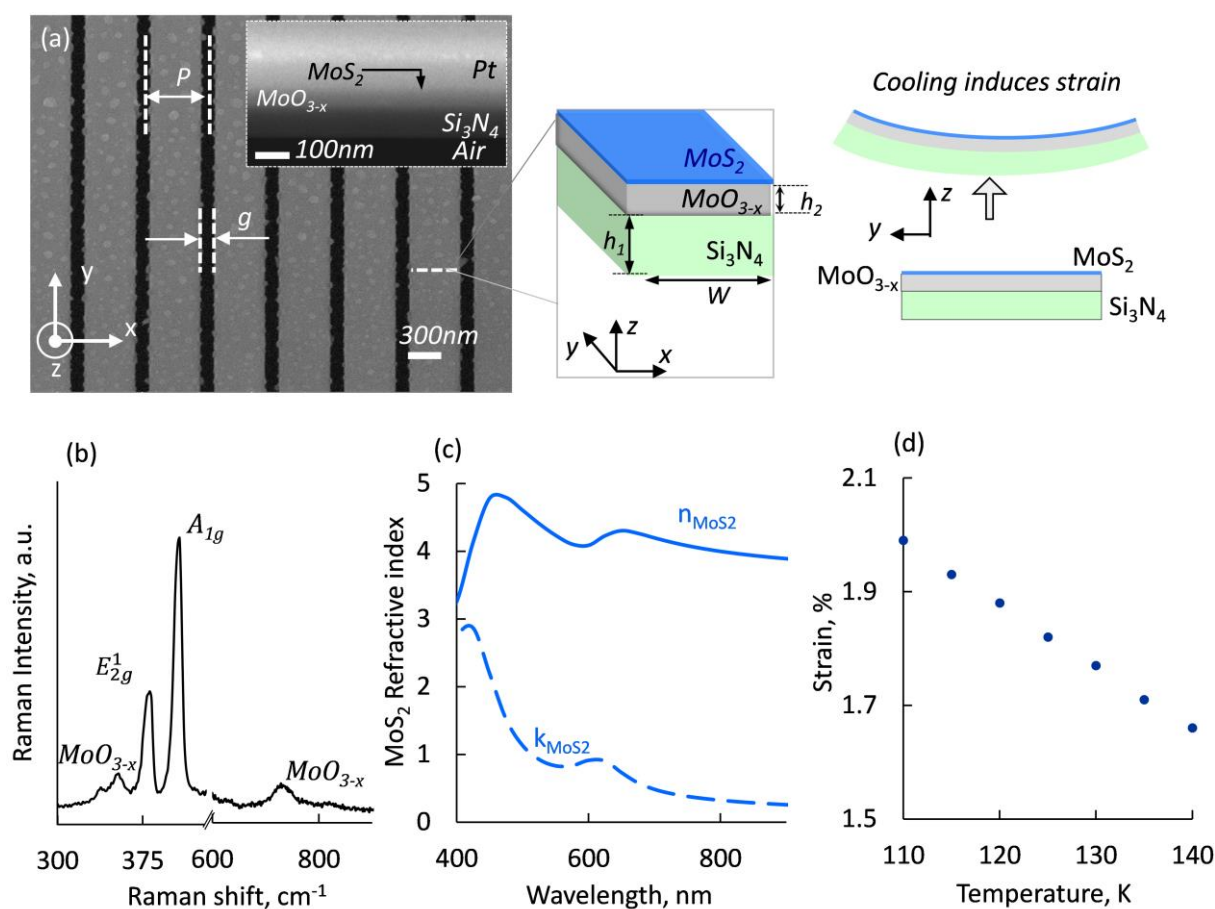
Figure 1. Mechanochromic metasurface. (a) Scanning electron microscope image of the metamaterial formed by a nanowire array manufactured on a $MoS_2/MoO_{3-x}/Si_3N_4$ trilayer free-standing membrane, schematic of a single nanowire [P = 500, g=100, h_1 = 90, h_2 = 50, h_3 = 5, W = 400nm], scale bar 300nm. Inset: cross section of the trilayer sample, coated with platinum to improve contrast. (b) Raman spectra of metamaterial shows the composition of the sample; (c) Ellipsometric data of a few layer MoS_2 film; (d) Strain induced in a single nanowire upon cooling, deformation of the nanowire is caused by the large thermal expansion mismatch between Si_3N_4 and MoO_{3-x}.
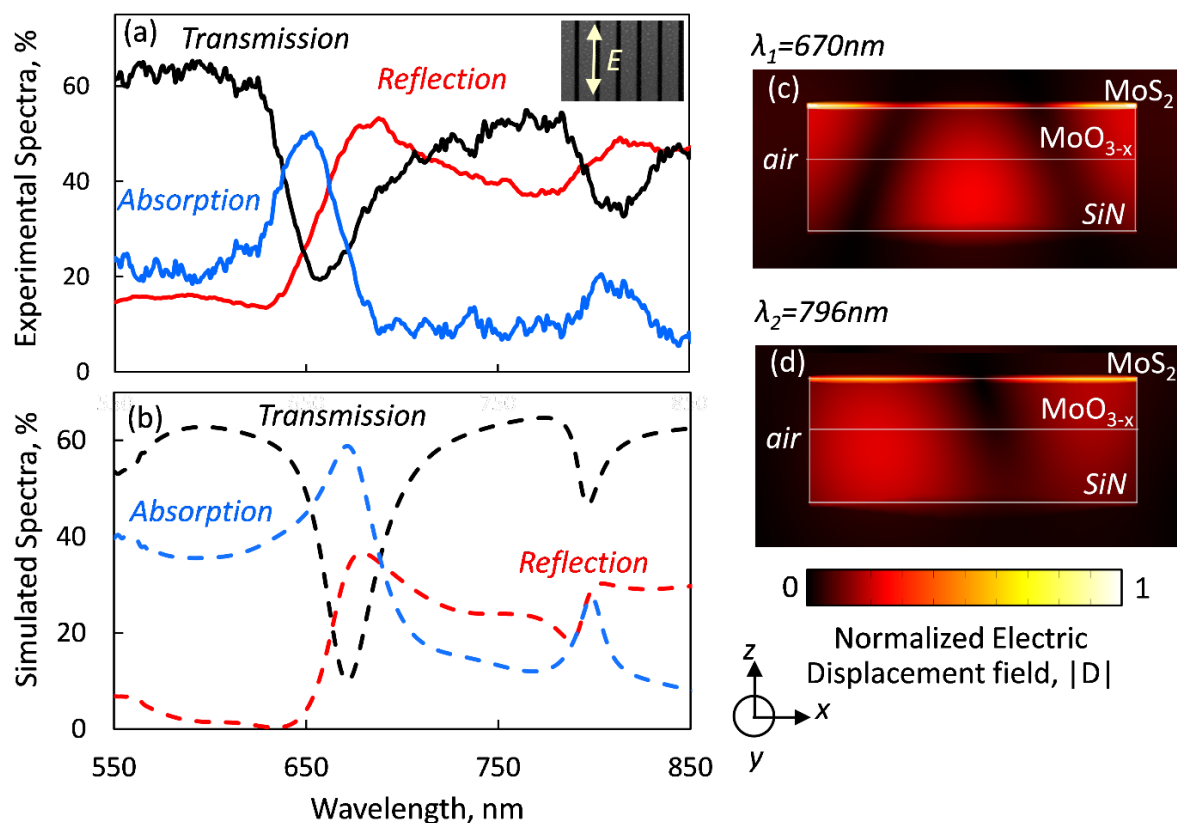
Figure 2. Optical properties of mechanochromic metasurface. (a) Reflection, transmission and absorption spectra of mechanochromic metamaterial under linear polarized illumination, as indicated on inset to plate. (b) Numerically simulated reflection, transmission and absorption spectra of the metamaterial. (c,d) Numerically simulated distribution of the electromagnetic field in the metamaterial nanowire. Color maps show the magnitude of the electric displacement field in the x-z plane.
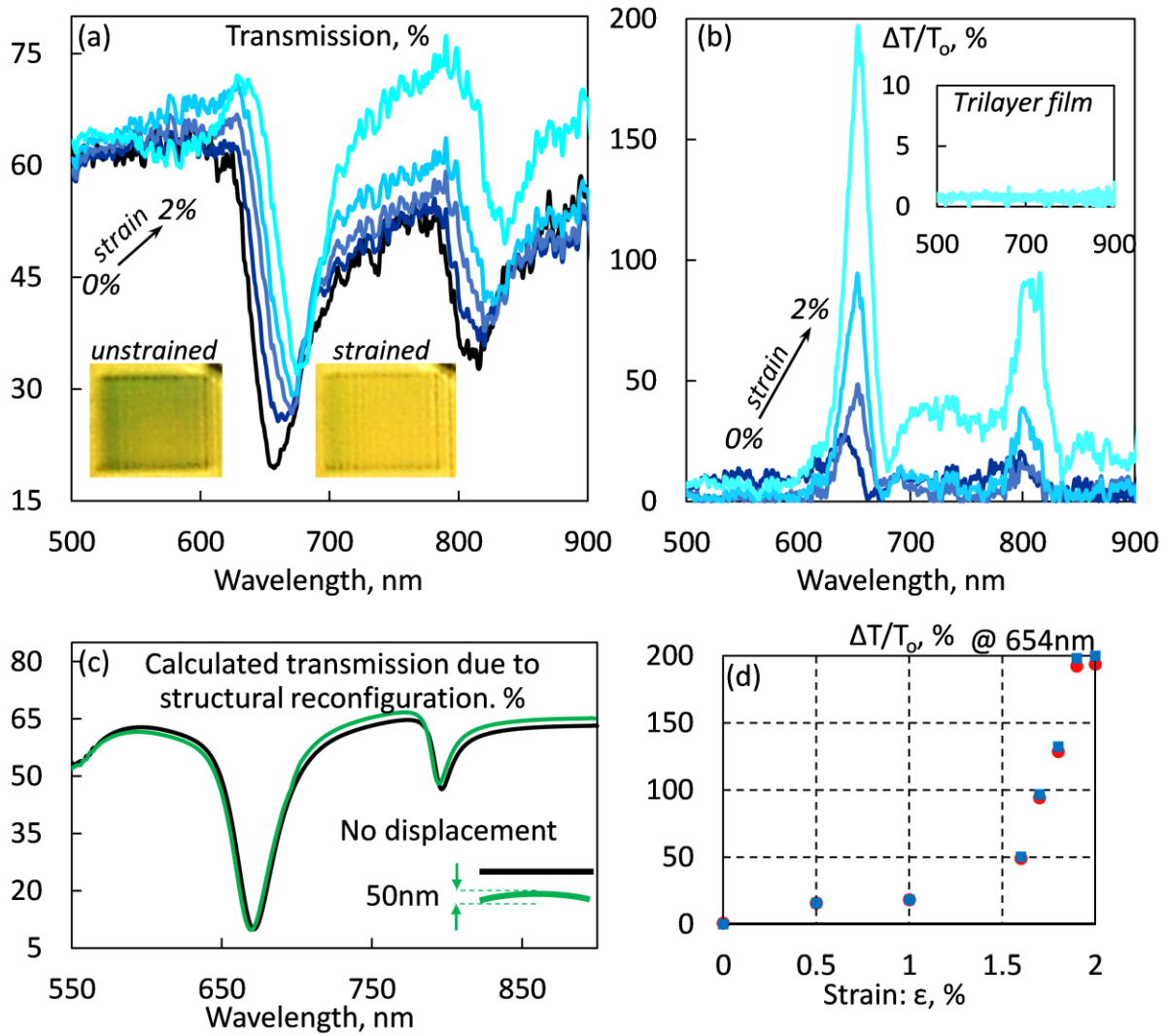
Figure 3. Mechanochromic reconfigurable metasurface. Variation of the optical properties of MoS$_2$ metamaterial under stress caused by slow cooling [5K/min]. (a) Spectral dispersion of transmission of the metamaterial for different levels of strain up to maximum strain of 2%. Insets shows the perceived colours of metamaterial sample for zero and 2% strain. (b) Relative transmission change for different strain levels. Inset: transmission change of the reference trilayer film. c) Calculated transmission of no displacement, black and 50nm displacement of the central part of the sample, green, assuming only structural reconfiguration and no stress dependent refractive index of the nanostructure. (d) Reversibility of induced mechanochromic effect- at 654nm- for the full strain cycle, strain up-red circular markers, strain down-cyan rectangular markers.
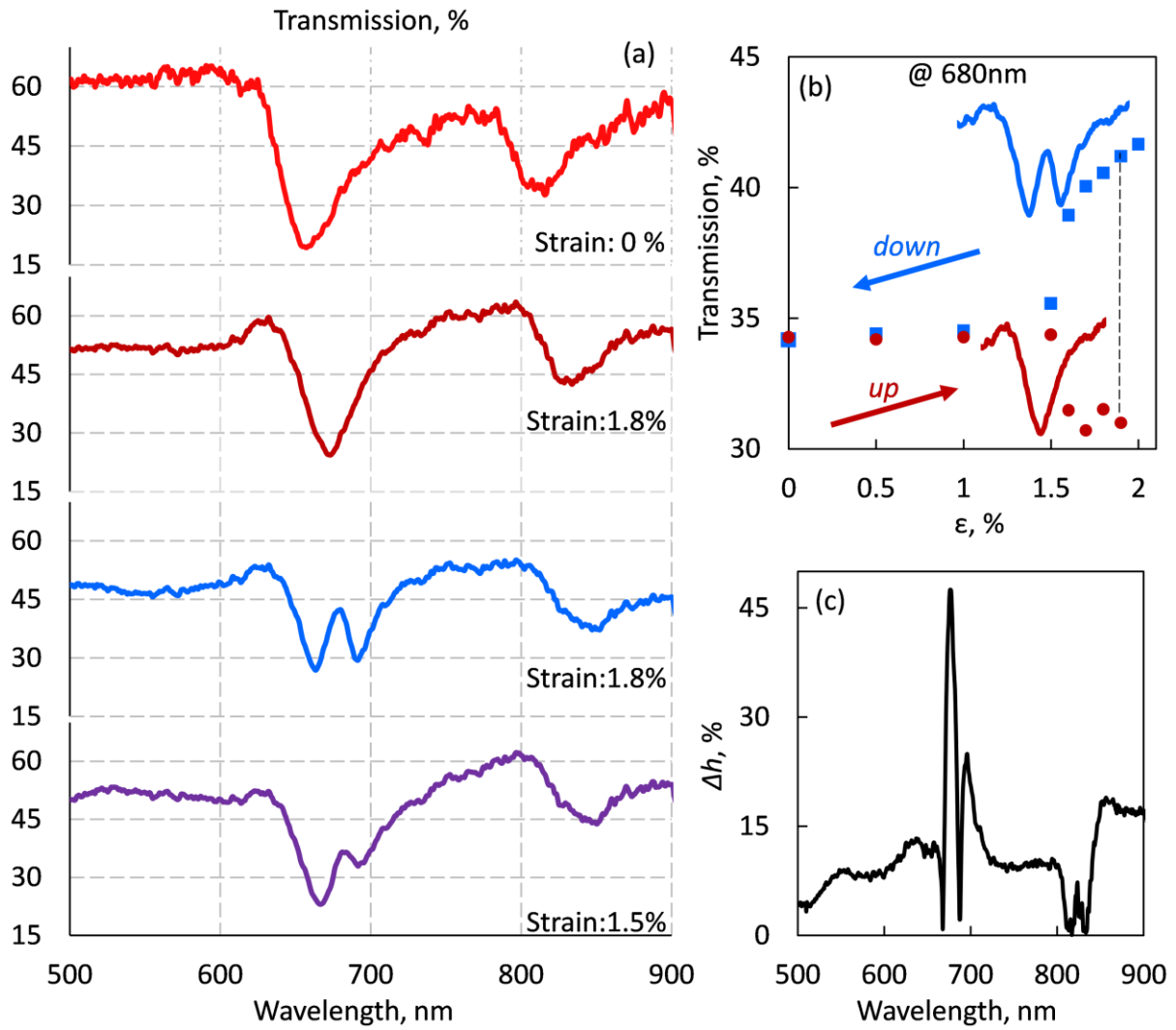
Figure 4. Hysterisis of mechanochromic metasurface. (a) Transmission spectra for different strain levels in the regime of rapid cooling [15K/min] (b) Variation of the metamaterial transmission at 680nm during the full strain cycle. A hysteresis of optical properties is observed at strain levels exceeding 1.5%. (c) Span of the hysteresis loop, Differential Hysteresis:$\Delta h=$ $|Tr_{up}(\lambda)-Tr_{down}(\lambda)|/Tr_{up}(\lambda)$ as a function of wavelength at strain level of 1.8%.